Enhancement of thermoelectric efficiency in triple quantum dots by the Dicke effect

Qiang Wang,[1] Haiqing Xie,[1] Yi-Hang Nie,[1,*] and Wei Ren[2,3,†]

[1]*Institute of Theoretical Physics and Department of Physics, Shanxi University, Taiyuan 030006, China*

[2]*Department of Physics, Shanghai University, 99 Shangda Road, Shanghai 200444, China*

[3]*Physics Department and Institute for Nanoscience and Engineering, University of Arkansas, Fayetteville, Arkansas 72701, USA*

(Received 6 November 2012; published 4 February 2013)

We theoretically study thermoelectric transport through a quantum dot coupled to two side quantum dots in the linear response regime by the nonequilibrium Green's function technique. Our results show that thermoelectric properties are strongly influenced by the Dicke effect. At low temperature, for small (very large) level shift and large interdot coupling the subradiant state contributes a sharp peak to the Dicke spectral line in the electrical and thermal conductance spectrum and leads to a strong violation of the Wiedemann-Franz law. As a result, the thermoelectric efficiency is strongly enhanced near the subradiant state. At relatively high temperature, the large tunneling coupling may be used to compensate the attenuation of the interference effect so that a considerable thermoelectric efficiency can still be obtained around the subradiant state. Moreover, the thermoelectric efficiency is also strongly dependent on the asymmetry parameter and intradot Coulomb interaction.

DOI: 10.1103/PhysRevB.87.075102 PACS number(s): 73.50.Lw, 65.80.−g, 85.80.Lp, 73.63.Kv

I. INTRODUCTION

Recently, due to the potential for applications of highly efficient thermoelectric devices, thermoelectric effects in quantum dot (QD) systems have been widely studied both experimentally[1–5] and theoretically.[6–22] The thermoelectric efficiency in QD systems can achieve considerable values due to strong violation of the Wiedemann-Franz (WF) law[6,7] and small phonon contribution to thermal conductance.[8–10] From the experiment point of view, the parameters of QD systems are more easily controlled, which suggests that QD systems are promising candidates for better thermoelectric devices. On the other hand, many novel thermoelectric phenomena have been observed or predicted in QD systems. For example, Coulomb blockade oscillations of the thermopower and the thermal conductance were obtained for Coulomb islands with the gate voltage.[2,11,12] The bipolar effect in the thermal conductance spectrum at high temperature has been observed in multilevel QD systems[15] and serial-coupled double quantum dot (DQD).[16,17] In addition, the spin Seebeck effect was also observed in QD systems with ferromagnetic electrodes.[19–22]

Electron transport through multiple QD systems exhibits a variety of interesting interference effects,[23–26] such as Aharonov-Bohm (AB), Fano, and Dicke effects. More recently, some works have concerned the interplay between the thermoelectric effects and the interference effects.[27–36] For a QD embedded in an AB ring, the interference effect results in AB oscillations of the thermopower due to the modulation of the magnetic flux.[29] Theoretical studies show that the interference effects can strongly influence the thermoelectric coefficients in parallel-coupled DQD systems by tuning the asymmetry of dot-lead coupling and the magnetic flux. Since the thermopower is extremely sensitive to the slope of the transmission function in the vicinity of Fermi level, a large enhancement of thermoelectric efficiency by Fano effect have been obtained.[30,32,35,36] The coupled triple quantum dot (TQD) systems have more complex geometrical configuration and more tunable parameters, and the electronic transport through them can exhibit various interference behaviors,[37–41] which can be used to improve thermoelectric efficiency of the systems. However, to the best of our knowledge, up to now thermoelectric transport through TQD system remains less studied, particularly taking into account the influence of the interference effects.

The Dicke effect in quantum optics means the presence of a strong and narrow spontaneous emission line in addition to much broader lines of a collection of atoms, which are separated by a distance smaller than the wavelength of the emitted light.[42] The Dicke effect in the mesoscopic system was first predicted in two-channel resonant tunneling,[43] since then the analogies to the Dicke effect have been found in some other mesoscopic systems. In a coupled DQD system under a magnetic field, the conductance shows Dicke effects that can be controlled by the magnetic flux.[44] The properties of transmission spectrum and the local density of states (LDOS) in a QD side coupled to a quantum wire can also be attributed to the electronic Dicke effect.[45] More recently, the Dicke effect has been predicted in a QD coupled to two side QDs structure in the Coulomb blockade regime[46] and Kondo regime,[47,48] in which the effective coupling between localized levels and a conduction channel gives rise to effectively fast supertunneling and slow subtunneling modes. Since the LDOS can exhibits almost a δ-like shape for appropriate parameters due to the Dicke effect, one expects a significant enhancement of the thermal efficiency.

In this paper we present a systematic investigation of the influence of the Dicke effect on the thermoelectric transport through a TQD system. The basic thermoelectric coefficients in the linear response regime are obtained by the nonequilibrium Green's function technique. Our results show that at low temperature, the electrical and thermal conductances exhibit characteristics of the Dicke effect, which can be used to improve the thermoelectric properties of the system. Small (or very large) level shift and large interdot coupling may enhance thermoelectric efficiency near the subradiant state, where density of states almost exhibits a δ-like shape, due to a strong violation of the WF law. With increasing temperature the interference effect is weakened, however, the attenuation can be compensated by enhancing tunneling coupling so that considerable figure of merit is still obtained near the subradiant state for large interdot coupling. Moreover, the influence of the

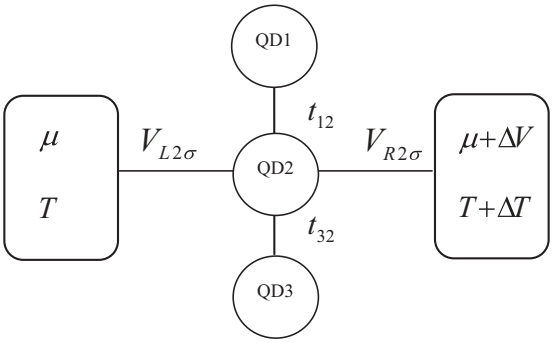

FIG. 1. A schematic picture of a QD (QD2) coupled to two metal leads and to two side QDs (QD1 and QD3).

asymmetry parameter and the interdot Coulomb interaction will also be discussed.

The rest of this work is organized as follows. In Sec. II, we introduce the model of a QD side coupled to two QDs and derive the basic analytical formulas. In Sec. III, we present the corresponding numerical results in detail. Finally, In Sec. IV we summarize the work.

II. MODEL AND FORMALISM

The system under consideration consists of a central QD (QD2) coupled to two metal leads and to two side QDs (QD1 and QD3), as shown schematically in Fig. 1, which can be described by a multi-impurity Anderson Hamiltonian as $H = H_l + H_d + H_T$. The first term is for the noninteracting electrons in the leads and written as $H_l = \sum_{\alpha=L,R}\sum_{k\sigma}\varepsilon_{k\alpha}c^\dagger_{k\alpha\sigma}c_{k\alpha\sigma}$, where $c^\dagger_{k\alpha\sigma}(c_{k\alpha\sigma})$ creates (annihilates) an electron with energy $\varepsilon_{k\alpha}$, momentum k, and spin σ in the lead α. The second term of Hamiltonian describes the TQD and takes the form[46,47]

$$H_d = \sum_{m\sigma}\varepsilon_{m\sigma}d^\dagger_{m\sigma}d_{m\sigma} + U\sum_m n_{m\sigma}n_{m\bar{\sigma}} - \sum_\sigma\sum_{j=1,3}[t_{j2}d^\dagger_{1\sigma}d_{2\sigma} + \text{H.c.}], \quad (1)$$

where $d^\dagger_{m\sigma}$ ($d_{m\sigma}$) denotes the creation (annihilation) operator of an electron with spin σ in QDm ($m = 1,2,3$). We assume that each QD has only a single energy level $\varepsilon_{m\sigma}$. $n_{m\sigma} = d^\dagger_{m\sigma}d_{m\sigma}$ is the electron number operator in QDm. U indicates the strength of intradot Coulomb interaction and the interdot Coulomb interaction is negligible. t_{j2} ($j = 1,3$) describes the tunneling coupling between two side QDs and the central QD2. The last term H_T describes the tunneling coupling between the central QD2 and the electrodes, and can be expressed as $H_T = \sum_{k\alpha\sigma}(V_{\alpha 2\sigma}c^\dagger_{k\alpha\sigma}d_{2\sigma} + \text{H.c.})$, where $V_{\alpha 2\sigma}$ is the tunneling matrix element between the central QD2 and the electrode α.

Using the nonequilibrium Green's function technique, we can calculate the electric and heat currents flowing from the left lead to the right with the formulas

$$I = \sum_\sigma\frac{e}{\hbar}\int\frac{d\omega}{2\pi}[f_L(\omega) - f_R(\omega)]T_\sigma(\omega), \quad (2)$$

$$I_Q = \sum_\sigma\frac{1}{\hbar}\int\frac{d\omega}{2\pi}(\omega-\mu_\alpha)[f_L(\omega) - f_R(\omega)]T_\sigma(\omega), \quad (3)$$

where $f_\alpha = [e^{(\omega-\mu_\alpha)/k_BT_\alpha}+1]^{-1}$ is the Fermi distribution function in the lead α with chemical potential μ_α and temperature T_α. $T_\sigma(\omega)$ is the transmission function of electron with spin index σ, and is given by $T_\sigma(\omega) = \text{Tr}[G^a_\sigma(\omega)\Gamma^\sigma_R G^r_\sigma(\omega)\Gamma^\sigma_L]$, where $\Gamma^\sigma_\alpha(\alpha = L,R)$ is the linewidth matrix with the matrix element defined as $\Gamma^\sigma_{nm\alpha} = V_{\alpha n\sigma}V^*_{\alpha m\sigma}\sum_k 2\pi\delta(\omega-\varepsilon_{k\alpha})$. In the wide-band limit, Γ^σ_α is independent of the energy and has the form

$$\Gamma^\sigma_\alpha = \begin{pmatrix}0&0&0\\0&\Gamma^\sigma_{22\alpha}&0\\0&0&0\end{pmatrix}. \quad (4)$$

Besides, $G^{r,a}_\sigma(\omega)$ are the retarded and advanced Green's functions in the frequency space. By using the equation of motion method and adopting the Hartree-Fock truncating approximation, we can calculate the retarded Green's function from the Dyson equation[41]

$$G^r_\sigma(\omega) = g^r_\sigma(\omega) + g^r_\sigma(\omega)\Sigma^r_\sigma G^r_\sigma(\omega), \quad (5)$$

where the self-energy can be expressed as $\Sigma^r_\sigma = -\frac{i}{2}[\Gamma^\sigma_R + \Gamma^\sigma_L]$, and $g^r_\sigma(\omega)$ is the retarded Green's function of the isolated QD without coupling to leads and can be given by

$$g^r_\sigma(\omega) = \begin{bmatrix}C_{11}&t_{12}&0\\t_{12}&C_{22}&t_{32}\\0&t_{32}&C_{33}\end{bmatrix}^{-1}, \quad (6)$$

where $C_{m\sigma} = (\omega-\varepsilon_{m\sigma}-U)(\omega-\varepsilon_{m\sigma})/(\omega-\varepsilon_{m\sigma}-U+Un_{m\bar{\sigma}})$ with $n_{m\bar{\sigma}} = \langle d^\dagger_{m\bar{\sigma}}d_{m\bar{\sigma}}\rangle$. The average electron occupation number in QDm can be calculated self-consistently by the relation $n_{m\bar{\sigma}} = -i\int\frac{d\omega}{2\pi}G^<_{mm\bar{\sigma}}(\omega)$, in which the lesser Green's function $G^<_\sigma(\omega)$ can be calculated from the Keldysh equation $G^<_\sigma(\omega) = G^r_\sigma(\omega)\Sigma^<_\sigma(\omega)G^a_\sigma(\omega)$ with the lesser self-energy $\Sigma^<_\sigma(\omega) = i[f_L(\omega)\Gamma^\sigma_L + f_R(\omega)\Gamma^\sigma_R]$, while the advanced Green's function $G^a(\omega)$ can be obtained via a relation $G^a(\omega) = [G^r(\omega)]^\dagger$. Note that the operating temperature for the above calculation should be restricted in the region higher than the Kondo temperature.

In the linear response regime, the electric and heat currents through the system can be transformed to the following form

$$I = e^2L_0\Delta V + \frac{eL_1}{T}\Delta T, \quad (7)$$

$$I_Q = -eL_1\Delta V - \frac{L_2}{T}\Delta T \quad (8)$$

with $L_n = -\sum_\sigma\frac{1}{\hbar}\int\frac{d\omega}{2\pi}(\omega-\mu)^n\frac{\partial f(\omega,\mu,T)}{\partial\omega}T_\sigma(\omega)$. On the basis of linear response, the chemical potential and temperature in two leads satisfy the relation $\mu_L = \mu_R$, $T_L = T_R = T$. The electrical and thermal conductances can be calculated as $G = e^2L_0$ and $\kappa_e = \frac{1}{T}[L_2 - \frac{L_1^2}{L_0}]$, respectively. The thermopower is defined as $S = \frac{\Delta V}{\Delta T} = -\frac{1}{eT}\frac{L_1}{L_0}$. And the efficiency of heat-electricity conversion of the system is described by the dimensionless figure of merit $ZT = \frac{GS^2T}{\kappa_e+\kappa_{\text{ph}}}$, where κ_{ph} is the phonon contribution to the thermal conductance. In QDs systems, the heat current carried by phonons can be blocked effectively by some particular materials or designs,[1,4,8–10] for example, adding a vacuum layer between the tunneling

junction. So in the following calculation we ignore the influence of $\kappa_{\rm ph}$.

III. NUMERICAL RESULTS

In the following we assume that QD levels are independent of electron spin and chosen as $\varepsilon_1 = \varepsilon - \Delta$, $\varepsilon_2 = \varepsilon$, $\varepsilon_3 = \varepsilon + \Delta$, where Δ describes the level spacing between two side QDs and the central QD, and the parameters of the leads are $\mu_L = \mu_R = 0$. Based on the above formulas, we carry out the numerical calculation to investigate thermoelectric transport through the TQD system. The couplings between the central dot and the leads, $\Gamma^{\sigma}_{22L} = \Gamma^{\sigma}_{22R} = \Gamma$, are generally used as the energy unit. In typical QDs, Γ can reach approximately the order of meV. In addition, we introduce a new parameter $\alpha = t_{12}/t_{32}$, which describes the asymmetry of the couplings of two side QDs to the central QD. Since the properties of the thermoelectric transport through the system depend on the level shift Δ, the interdot tunneling coupling t and Coulomb interaction U, our discussions will be presented according to the influences of these three major tuning parameters.

A. Influence of level shift

First we consider the case of fixed interdot tunneling coupling and vanishing Coulomb interaction. The couplings between two side QDs to the central QD are set to be symmetric, i.e., $\alpha = 1$ and $t_{32} = t_{12} = t$. We first consider the low-temperature regime. In Fig. 2, the thermoelectric quantities are plotted as a function of the level ε for several values of Δ with $k_B T = 0.01\Gamma$. The dependence of the electronic Dicke effect in conductance spectrum on Δ is shown in Fig. 2(a), which is consistent with the results in Ref. 46, where the central dot couples to two ferromagnetic leads. In the low-temperature regime, the behavior of electrical conductance is determined by the transmission function

$$T(\omega) = \frac{[\tilde{\omega}^2 - \Delta^2]^2\Gamma^2}{[\tilde{\omega}^2 - \Delta^2 - 2t^2]^2\tilde{\omega}^2 + \Gamma^2[\tilde{\omega}^2 - \Delta^2]^2}, \qquad (9)$$

where $\tilde{\omega} = \omega - \varepsilon$. Equation (9) shows that in the transmission function there are three resonant peaks appearing at $\tilde{\omega} = \pm\sqrt{\Delta^2 + 2t^2}$, $\tilde{\omega} = 0$ and two zeros located at $\tilde{\omega} = \pm\Delta$ due to the quantum destructive interference effect, resulting in two antiresonance points in spectrum of electrical conductance. The width of resonant peaks is determined by the effective coupling between local levels and leads, which changes with variation of Δ. For $\Delta = 0$, the central QD can be equivalent to decoupling from the leads, leading to the vanishing of the central peak. For very small (but nonzero) values of Δ, the width of the central peak becomes much narrower. The narrow central peak arises from the subradiant state, whereas the other two wide peaks from corresponding superradiant states. With Δ increasing, the width of the central peak increases, while the one of two satellite peaks decreases. It can be clearly seen that the subradiant mode can transform to superradiant mode by tuning Δ. For very large level shift, two side peaks are much narrower while the central peak is wide. At low temperature, the thermal conductance is mainly dominated by the contribution of electron and thus depends on the transmission function. As a result, Dicke effect also appears

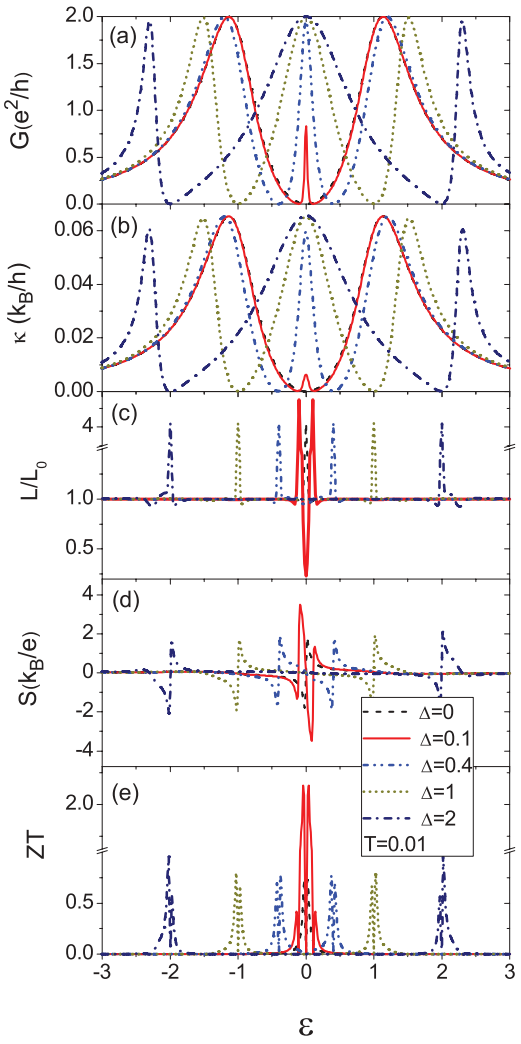

FIG. 2. (Color online) (a) Electrical conductance, (b) thermal conductance, (c) Lorentz ratio, (d) thermopower, and (e) figure of merit as a function of level position ε for different level shift Δ with $k_B T = 0.01\Gamma$. Other parameters are chosen as $\alpha = 1, t = 0.8\Gamma$, $U = 0$, and $\Gamma = 1$ meV.

in the spectrum of thermal conductance due to the quantum interference, as shown in Fig. 2(b), which exhibits similar behavior as the one of the electrical conductance. In order to clearly see the influence of Dicke effect on thermoelectric properties, we compare Lorentz ratio $L = \kappa/GT$ with Lorentz number $L_0 = (k_B\pi)^2/3e^2$ in Fig. 2(c). It can be found from Fig. 2(c) that Lorentz ratio strongly deviates from Lorentz number in the vicinity of antiresonance, indicating strong violation of the WF law. In particular, for small level shift ($\Delta \sim 0$) and very large level shift ($\Delta \gg \sqrt{2}t$), the Dicke effect is more pronounced, and L also deviates from L_0 in the vicinity of subradiant state. Since the subradiant state and the antiresonance points are close to each other, a strong violation of the WF law can be obtained.

The quantum interference has a significant impact on the thermopower S and figure of merit ZT as well. The thermopower S, shown in Fig. 2(d), has five zero points corresponding to three resonant points and two antiresonance points in the spectrum of electrical conductance. The magnitude

of S changes sign whenever ε passes a zero point, which is similar to the case of the single QD and DQD systems.[15,20,32,35] When the level ε is above one of these zero points the main carriers are electrons and then the thermopower is negative. When ε is below the zero point the main carriers are holes and thus the thermopower is positive. The considerable enhancement of the thermopower appears in the vicinity of the antiresonance points since the transmission function changes sharply near these points. For very small (or very large) Δ, the thermopower also changes sharply near the subradiant state and the density of states exhibits a δ-like shape. Because the subradiant state and the antiresonance points are close to each other, the thermopower is strongly enhanced. The property of the figure of merit ZT is shown in Fig. 2(e). When $\Delta = 0$, ZT presents only one single double-peak structure near $\varepsilon = 0$. For nonzero Δ, the spectrum of ZT is mainly dominated by two double-peak structures in the vicinity of the antiresonance points on both sides of Fermi level. Both peaks in each double-peak structure have different Δ dependence: the peak farther away from Fermi level decreases with decreasing Δ, whereas the one close to Fermi level increases. These behaviors are consistent with the variation of the slope of the transmission function. The degree of asymmetry of the double-peak structure in the ZT spectrum is also changed with the transition of resonant peaks from subradiant to superradiant mode. It is obvious that for small level shift $\Delta \sim 0$ (or very large level shift $\Delta \gg \sqrt{2}t$), the thermoelectric efficiency is significantly enhanced near the subradiant state where the WF law is strongly violated.

As is well known, the thermoelectric coefficients are strongly dependent on the temperature. In Fig. 3 we show the thermoelectric quantities as a function of ε at different temperature. With increasing temperature the interference effect is weakened. As shown in Figs. 3(a) and 3(b), Dicke resonance (central peak) is strongly suppressed and the antiresonance points in the electrical (thermal) conductance disappear. At high temperature, due to broadening of Fermi distribution function, more states participate in the heat transport, as a result the central narrow peak of κ at low temperature changes to a minimum (a valley) at high temperature, and meanwhile, on both sides of the minimum the two local maxima appear at the positions where the electrical conductances are minima, which can be attributed to local bipolar effect. In Fig. 3(c), we show L/L_0 as a function of ε at different temperature. It can be clearly seen that the increase of the temperature extends the range of the violation of the WF law. The behaviors are helpful for obtaining large thermopower and figure of merit in a large level range. At high temperature the maximum L appears at the locations where the thermal conductance presents local maximum and the magnitude decreases with increasing T. The magnitude of thermopower S and figure of merit ZT, shown in Figs. 3(d) and 3(e), first increase to achieve the largest value, and then decrease with increasing temperature. Both peaks of S and ZT become broader and flat with increasing T due to broadening of Fermi distribution function. Interestingly, at relatively high temperature ($k_BT = 0.1\Gamma$), the maxima of thermopower appear near the positions where the thermal conductance presents the local minimum and thus the maximum of the spectrum of ZT occurs at these positions. To show this more explicitly, we present the temperature

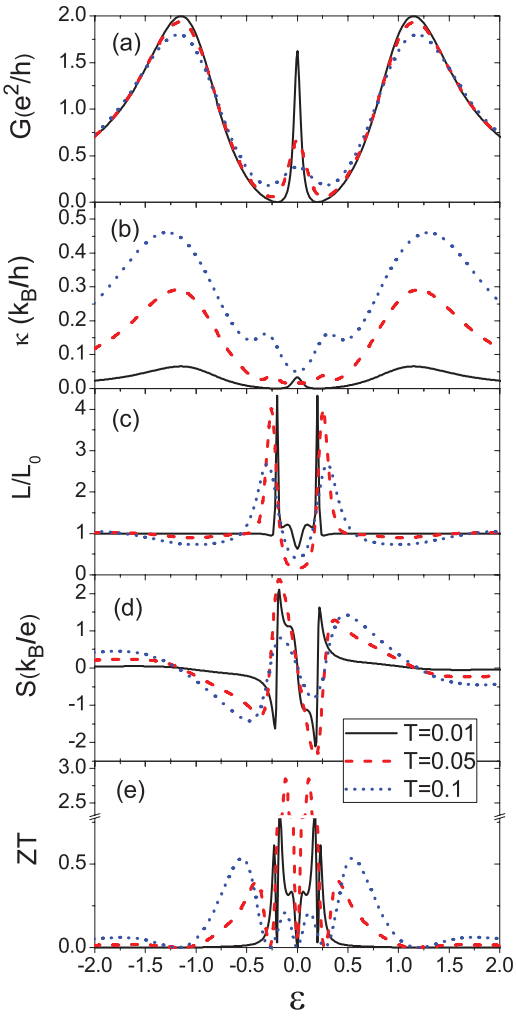

FIG. 3. (Color online) (a) Electrical conductance, (b) thermal conductance, (c) Lorentz ratio, (d) thermopower, and (e) figure of merit as a function of level position ε for different temperature with $\Delta = 0.2\Gamma$. Other parameters are the same as in Fig. 2.

and level position dependencies of ZT in Fig. 4. It can be clearly seen from Fig. 4 that ZT is significantly enhanced in the vicinity of the antiresonance points at relatively low temperature $k_BT \sim 0.05\Gamma$ and with increasing T, two peaks in the center gradually disappear while two side peaks start to dominate the spectrum.

As shown above, at relatively high temperature, the maximum of thermoelectric efficiency is suppressed. However, one also might expect a considerable thermal efficiency by tuning the level shift Δ. In Fig. 5(a) we present ZT versus the level position ε and the level shift Δ for $k_BT = 0.1\Gamma$. For relatively small (large) values of Δ, corresponding to the subradiant (superradiant) mode being located in the center while the superradiant (subradiant) modes being on both sides, ZT is mainly dominated by two side peaks located around the positions where the thermal conductance presents the local minimum. For large Δ ($>0.1\Gamma$) the positions of the side peaks in ZT change linearly with the variety of Δ. The intensities of side peaks increase monotonically with increasing Δ in a wide range of Δ and so a relatively large efficiency can be obtained at large Δ. To show the influence of Δ and

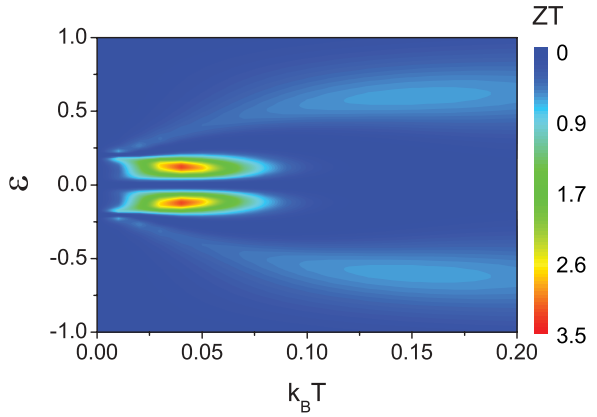

FIG. 4. (Color online) Figure of merit as functions of level position ε and temperature k_BT for $\Delta = 0.2\Gamma$, other parameters are taken as in Fig. 2.

T more explicitly, in Fig. 5(b) we present the temperature dependence of ZT for different Δ and corresponding ε near the antiresonance points. Nonmonotonic variation of ZT with temperature can be clearly observed. With increasing Δ, the temperature corresponding to the maximum of ZT first increases and then decreases. One can find from Fig. 5(b) that when interdot tunneling is fixed, in order to obtain large thermoelectric efficiency the appropriate match of Δ,ε, and

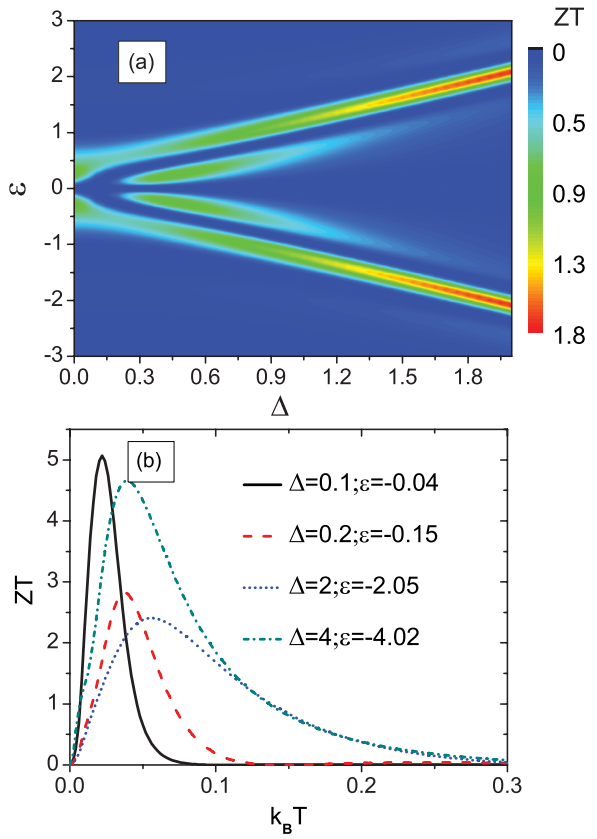

FIG. 5. (Color online) (a) Figure of merit ZT as functions of level position ε and the level shift Δ for $k_BT = 0.1\Gamma$. (b) ZT as a function of k_BT for indicated values of level position ε and level shift Δ. Other parameters are the same as in Fig. 2.

T is needed. ZT can present considerable value for very small and large Δ at appropriate low temperature ($k_BT < 0.05\Gamma$), and relatively large value for large Δ at relatively high temperature ($k_BT > 0.05\Gamma$), for optimizing condition of thermoelectric efficiency.

B. Influence of interdot tunneling

Next, we study the influence of interdot tunneling with fixed Δ. The interdot tunneling provides the channels that the quantum interference requires and may influence the interference effect by adjusting the effective coupling between local levels and leads, and then influence thermoelectric effects in TQD system. We first consider the case that the central QD couples symmetrically to side QDs. In Fig. 6, the thermoelectric quantities are plotted as a function of ε for several values of t at low temperature. The behaviors of thermoelectric coefficients with the variation of the interdot tunneling are analogous to the ones by changing the level shift. With increasing t, the central peak in the thermal conductance becomes narrow, while the satellite peaks become broad [see Fig. 6(a)]. However, the positions of the antiresonance points are unchanged. The transition from subradiant to superradiant

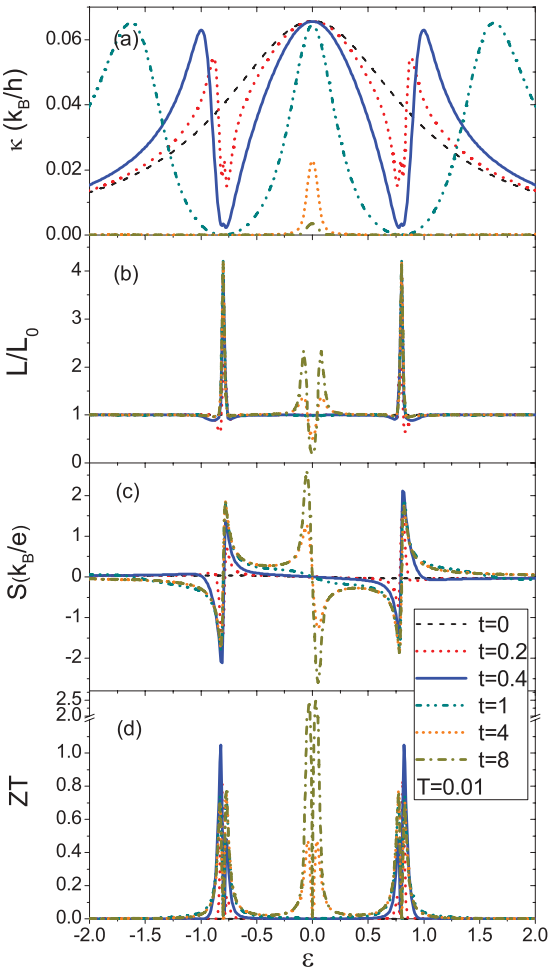

FIG. 6. (Color online) (a) Thermal conductance, (b) Lorentz ratio, (c) thermopower, and (d) figure of merit as a function of level position ε for different the interdot tunneling t with $\Delta = 0.8\Gamma$ and $k_BT = 0.01\Gamma$. Other parameters are the same as in Fig. 2.

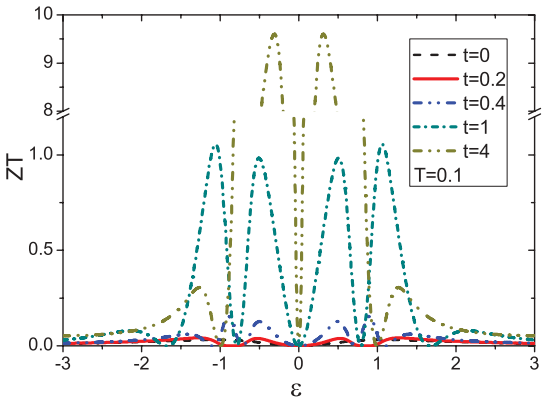

FIG. 7. (Color online) Figure of merit as a function of level position ε for different the interdot tunneling t with $\Delta = 0.8\Gamma$ and $k_BT = 0.1\Gamma$. Other parameters are the same as in Fig. 2.

mode can also be achieved by tuning the interdot tunneling. With increasing t, the central peak in thermal conductance changes from superradiant to subradiant state. It is obvious that a strong violation of the WF law emerges not only near antiresonance points but also near the subradiant state for large t, as shown in Fig. 6(b). The thermopower S and figure of merit ZT, shown in Figs. 6(c) and 6(d), are also strongly dependent on the interdot tunneling. For $t = 0$ the side QDs are decoupled to the central QD, the interference effect disappears and thermoelectric quantities S and ZT approach zero. When $t \neq 0$, electric Dicke effect emerges. For small t, the thermopower is strongly enhanced in the vicinity of the antiresonance points resulting in two high double-peak structures in the spectrum of ZT. With increasing t, the central peak in thermal conductance changes from superradiant to subradiant state. Meanwhile the thermopower starts to change sharply near this state where the WF law is also strongly violated. So a new double-peak structure appears in the ZT spectrum. In particular, for very large t the density of states around Fermi energy exhibits a δ-like shape, and then ZT is significantly enhanced. Although with increasing temperature the quantum interference is weakened so that ZT is attenuated, enhancing the tunneling coupling may compensate the attenuation. In Fig. 7 we present the dependence of ZT on the interdot tunneling at relatively high temperature ($k_BT = 0.1\Gamma$), which clearly shows ZT is suppressed for small interdot tunneling, but can be strongly enhanced near the central resonances point with large interdot tunneling. For very large interdot tunneling, ZT is mainly dominated by double peaks in the vicinity of the central resonances point, and can achieve considerable value (e.g., close to 10 for $t = 4\Gamma$). This is a consequence of the compensation of interference effect due to the interdot tunneling and due to the temperature. For the large interdot tunneling, the electronic interference effect is quite strong. In order to weaken the interference effect, a higher temperature is needed.

When $\alpha \neq 1$, the central QD asymmetrically couples to two side QDs. In Fig. 8, we present ZT as functions of level position ε and the asymmetry parameter α for two distinct temperature regimes: $k_BT = 0.01\Gamma$ and $k_BT = 0.1\Gamma$. It can be clearly seen that the thermoelectric efficiency is strongly influenced by the asymmetry parameter α due to the

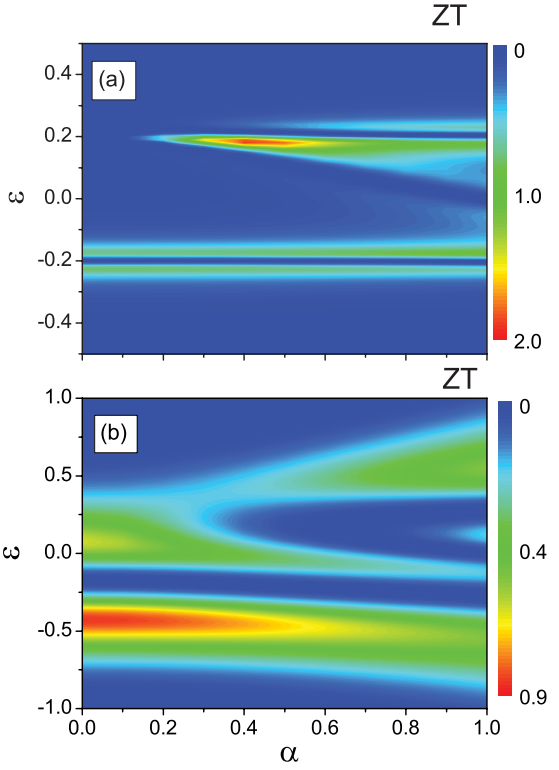

FIG. 8. (Color online) Figure of merit as a function of the level position ε and asymmetry parameter α, calculated for (a) $k_BT = 0.01\Gamma$ and (b) $k_BT = 0.1\Gamma$ for $\Delta = 0.2\Gamma$ and $t = 0.8\Gamma$. Other parameters are the same as in Fig. 2.

dependence of interference effects on α. Here the role of α is analogous to the asymmetry parameter of dot-lead coupling in parallel-coupled DQD systems.[32,35] At low temperature, the dependence of thermal conductance on α is similar to the one of electrical conductance, which has been shown in Ref. 46 (see Fig. 2 of Ref. 46). Thereby, here we only give a figure of ZT. When $\alpha = 0$, QD1 is decoupled from QD2 and two QDs form bondinglike and antibondinglike states, resulting in two resonant peaks in the electrical and thermal conductance spectra. An antiresonance point appears at $\varepsilon = -\Delta$ due to the quantum destructive interference and then ZT exhibits the typical double-peak structure around this point. It is interesting that the magnitudes of these peaks are almost invariable with increasing α [see Fig. 8(a)]. When $\alpha > 0$, a new sharp peak emerges in the conductance spectrum around the level of QD1. When $\alpha \sim 0.4$, a new antiresonance point starts to appear at $\varepsilon = \Delta$. Since the narrow peak and the new antiresonance point are closer to each other, ZT is significantly enhanced. With increasing α, the position of the narrow peak moves to Fermi level, and the thermoelectric efficiency decreases. When $\alpha = 1$, ZT is symmetrical with respect to $\varepsilon = 0$. When the temperature gets higher, the behavior of ZT becomes quite complex, as shown in Fig. 8(b). This complex behavior mainly comes from the complex behaviors of the thermal conductance and thermopower due to broadening Fermi distribution function. From the above results, at relatively high temperature, ZT will present peaks located at the positions where the thermal conductance presents the local minimum but the thermopower

presents local maximum. It is obvious that previous double peaks located near $\varepsilon = -\Delta$ appear at the high-energy position. At relatively high temperature, a relatively large thermoelectric efficiency can be obtained near $\alpha \sim 0$. When $\alpha \to 1$, the ZT spectrum also becomes symmetrical with respect to $\varepsilon = 0$.

C. Influence of intradot Coulomb interactions

Now we consider the impact of the intradot Coulomb interaction on the thermoelectric properties in the presence of Dicke effect. At low temperature the Coulomb interaction splits the Dicke spectral line into two sets, which give rise to the richer structure of the thermoelectric coefficients. In Fig. 9 we show thermoelectric quantities as a function of ε for different Coulomb interaction at $T = 0.01\Gamma$. For large U (e.g., $= 3\Gamma$) it is obvious that the Dicke spectral lines in the electrical and thermal conductance split into two sets and their centers are located at $\varepsilon = 0$ and U [see Figs. 9(a) and 9(b)]. When the Coulomb interaction $U \gtrsim 2\sqrt{\Delta^2 + 2t^2}$, the two sets of Dicke spectral line can be completely separated and are symmetric with respect to the electron hole symmetry point $\varepsilon = -U/2$. Besides four antiresonance points due to the quantum destructive interference, a new zero point of the conductance appears at the electron hole symmetry point. Thus a large deviation from the WF law appears near the electron hole symmetry point in comparison with the case in absence of Coulomb interaction, as shown in Fig. 9(c). Moreover, at the resonant points and zero points of the electrical conductance, the contributions of electrons to the current are compensated by the ones of holes, and thus the thermopower disappears and changes sign when the level passes these points, as shown in Fig. 9(d). The figure of merit is presented in Fig. 9(e), the spectrum of ZT is mainly dominated by five double-peak structures, of which four double peaks are near the antiresonance points, and one is near the the electron hole symmetry point. G, κ and ZT are all symmetric with respect to the electron hole symmetry point $\varepsilon = -U/2$, whereas S is antisymmetric. When U is small, the Dicke spectral line and its Coulomb counterpart overlap, leading to the complex characteristics of S and ZT. In particular, for an appropriate

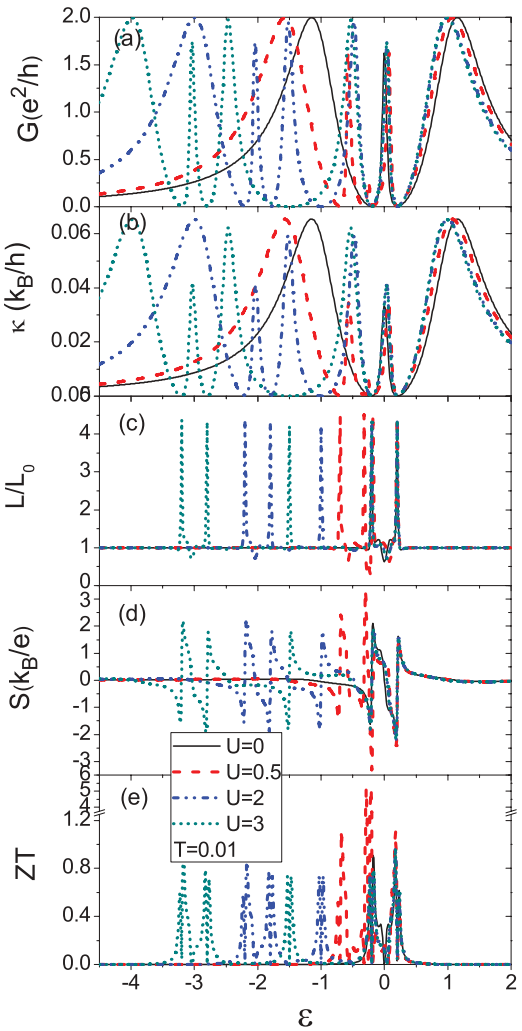

FIG. 9. (Color online) (a) Electrical conductance, (b) thermal conductance, (c) Lorentz ratio, (d) thermopower, and (e) figure of merit as a function of level position ε for different Coulomb interaction with $k_B T = 0.01\Gamma$ and $\Delta = 0.2\Gamma$. Other parameters are the same as in Fig. 2.

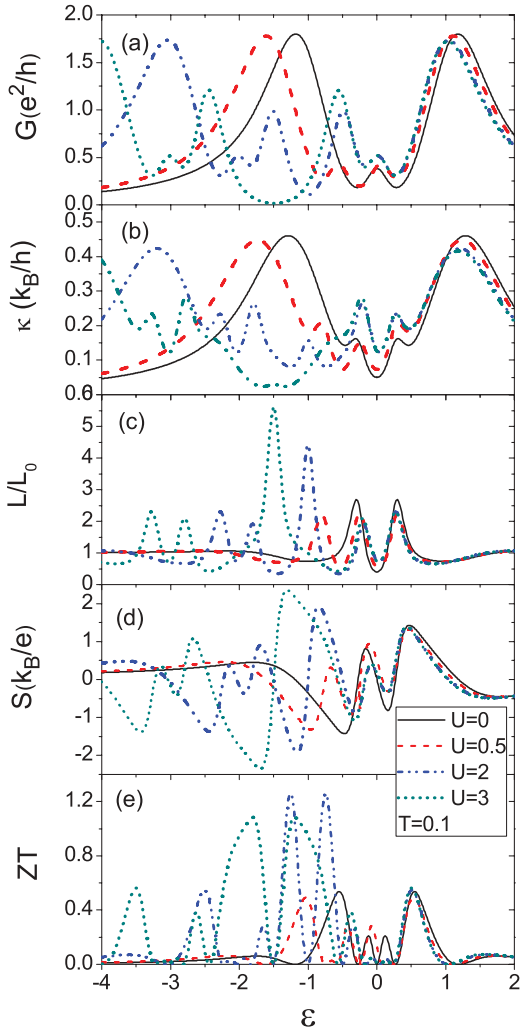

FIG. 10. (Color online) (a) Electrical conductance, (b) thermal conductance, (c) Lorentz ratio, (d) thermopower, and (e) figure of merit as a function of level position ε for different Coulomb interaction with $k_B T = 0.1\Gamma$ and $\Delta = 0.2\Gamma$. Other parameters are the same as in Fig. 9.

small U (for example, $U = 0.5\Gamma$), Dicke spectral line and its Coulomb counterpart are very close to each other so that the two adjacent peaks incorporate into a very sharp peak and lead to a strong violation of the WF law. Then the thermoelectric efficiency ZT is strongly enhanced.

The thermoelectric quantities as a function of ε for different Coulomb interaction at $T = 0.1\Gamma$ is presented in Fig. 10. The behaviors of electrical and thermal conductance with the variation of temperature are similar to the ones in the case with vanishing Coulomb interaction. At relatively higher temperature, since the quantum interference effect is suppressed, the antiresonance points of electrical and thermal conductance also disappear, see Figs. 10(a) and 10(b). However, the electrical conductance can approach to zero at the electron hole symmetry point for large Coulomb interactions ($U = 3\Gamma$), while the thermal conductance presents a tiny peak at the same point, which can be attributed to the bipolar effect.[15,16] Then these behaviors of electrical and thermal conductances determine the properties of the Lorentz ratio shown in Fig. 10(c). It is obvious that the magnitude of Lorentz ratio near the antiresonance points becomes smaller than the one at low temperature, but the magnitude near the the electron hole symmetry point becomes much larger. The behaviors of S and ZT, shown in Figs. 10(d) and 10(e), are quite complex with the variety of Coulomb interactions. For different Coulomb interactions, due to substantial modifications of the level spacing, the dependencies of thermoelectric coefficients on the temperature are quite different. However, for large Coulomb interactions an evident enhancement of the thermoelectric efficiency ZT can be obtained near the electron hole symmetry point due to a strong violation of the WF law.

IV. CONCLUSION

In summary, we theoretically study thermoelectric transport through a QD coupled with two side QDs. It is found that thermoelectric properties are strongly influenced by the Dicke effect which can be controlled by the level shift, interdot tunneling coupling, and Coulomb interaction. At low temperature, when two side QDs are symmetrically coupled to the central QD, the electrical and thermal conductance exhibit the electronic version of the Dicke effect. For very small (very large) level shift and large interdot tunneling coupling, thermoelectric efficiency is strongly enhanced near the subradiant state, where density of states exhibits a δ-like shape, due to a strong violation of the WF law. For an appropriate small Coulomb interaction, the Dicke spectral line and its Coulomb counterpart form a very sharp peak in the conductance spectrum and lead to a large enhancement of figure of merit. For the situation with asymmetrically coupled dots, the efficiency is significantly enhanced when the new antiresonance appears for medium value of asymmetry parameter. At relatively high temperature, although the interference effect is weakened, a large tunneling coupling may compensate the attenuation so that a considerable thermoelectric efficiency can still be obtained near the subradiant state. Moreover, the thermoelectric efficiency can also be enhanced near the electron hole symmetry point for appropriate Coulomb interaction. Finally, we give an estimation of the magnitude of the temperature used in our calculations. When Γ is chosen as 1 meV, which can be achieved experimentally in typical QDs, the corresponding low temperature is $k_B T = 0.01\Gamma \simeq 120$ mK and the corresponding relatively high temperature is $k_B T = 0.1\Gamma \simeq 1.20$ K. These temperatures are lower than room temperature but higher than the Kondo temperature, and consistent with the thermoelectric experimental parameter.[5] Moreover, following the estimation in Ref. 9, the phonon contribution to the thermal conductance is quite small and the thermal efficiency can be reduced by 12%.

ACKNOWLEDGMENTS

This work was supported by the National Nature Science Foundation of China (Grants No. 11274208, No. 10974124, No. 11004124, and No. 11274222), the Shanxi Nature Science Foundation of China (Grant No. 2009011001-1), and the Eastern Scholar Professorship at Shanghai Institutions of Higher Education, Shanghai Municipal Education Commission.

*nieyh@sxu.edu.cn
†weiren@uark.edu

[1] T. C. Harman, P. J. Taylor, M. P. Walsh, and B. E. LaForge, Science **297**, 2229 (2002).
[2] T. S. Kim and S. Hershfield, Phys. Rev. Lett. **88**, 136601 (2002).
[3] R. Scheibner, H. Buhmann, D. Reuter, M. N. Kiselev, and L. W. Molenkamp, Phys. Rev. Lett. **95**, 176602 (2005).
[4] P. Reddy, S. Y. Jang, R. A. Segalman, and A. Majumdar, Science **315**, 1568 (2007).
[5] R. Scheibner, M. Konig, D. Reuter, A. D. Wieck, H. Buhmann, and L. W. Molenkamp, New J. Phys. **10**, 083016 (2008).
[6] B. Kubala, J. König, and J. Pekola, Phys. Rev. Lett. **100**, 066801 (2008).
[7] P. G. Murphy, S. Mukerjee, and J. E. Moore, Phys. Rev. B **78**, 161406(R) (2008).
[8] D. Nozaki, H. Sevincli, W. Li, R. Gutierrez, and G. Cuniberti, Phys. Rev. B **81**, 235406 (2010).
[9] David M.-T. Kuo and Y. C. Chang, Phys. Rev. B **81**, 205321 (2010).
[10] M. Tsaousidou and G. P. Triberis, J. Phys.: Condens. Matter **22**, 355304 (2010).
[11] X. Zianni, Phys. Rev. B **75**, 045344 (2007).
[12] X. S. Chen, H. Buhmann, and L. W. Molenkamp, Phys. Rev. B **61**, 16801 (2000).
[13] M. Wierzbicki and R. Świrkowicz, J. Phys.: Condens. Matter **22**, 185302 (2010).
[14] A. Crepieux, F. Simkovic, B. Cambon, and F. Michelini, Phys. Rev. B **83**, 153417 (2011).
[15] J. Liu, Q. F. Sun, and X. C. Xie, Phys. Rev. B **81**, 245323 (2010).
[16] F. Chi, J. Zheng, X. D. Lu, and K. C. Zhang, Phys. Lett. A **375**, 1352 (2011).

[17]D. M. T. Kuo and Y. C. Chang, Jpn. J. Appl. Phys. **50**, 105003 (2011).
[18]David M.-T. Kuo, S. Y. Shiau, and Y. C. Chang, Phys. Rev. B **84**, 245303 (2011).
[19]Y. Dubi and M. Di Ventra, Phys. Rev. B **79**, 081302(R) (2009).
[20]R. Świrkowicz, M. Wierzbicki, and J. Barnaś, Phys. Rev. B **80**, 195409 (2009).
[21]M. Wierzbicki and R. Świrkowicz, Phys. Rev. B **82**, 165334 (2010); Phys. Lett. A **375**, 609 (2011).
[22]J. Zheng and F. Chi, J. Appl. Phys. **111**, 093702 (2012).
[23]M. L. Ladron de Guevara, F. Claro, and P. A. Orellana, Phys. Rev. B **67**, 195335 (2003).
[24]H. Z. Lu, R. Lü, and B. F. Zhu, Phys. Rev. B **71**, 235320 (2005).
[25]P. Trocha and J. Barnaś, Phys. Rev. B **76**, 165432 (2007).
[26]D. Loss and E. V. Sukhorukov, Phys. Rev. Lett. **84**, 1035 (2000).
[27]Z. Y. Zhang, J. Phys.: Condens. Matter **19**, 086214 (2007).
[28]R. Franco, J. S. Valencia, and M. S. Figueira, J. Appl. Phys. **103**, 07B726 (2008).
[29]Y. M. Blanter, C. Bruder, R. Fazio, and H. Schoeller, Phys. Rev. B **55**, 4069 (1997).
[30]Y. S. Liu and X. F. Yang, J. Appl. Phys. **108**, 023701 (2010).
[31]Y. S. Liu, D. B. Zhang, Xi. Feng. Yang, and J. F. Feng, Nanotechnology **22**, 225201 (2011)
[32]M. Wierzbicki and R. Świrkowicz, Phys. Rev. B **84**, 075410 (2011).
[33]Z. P. Niu, Eur. Phys. J. B **82**, 153 (2011).
[34]O. Karlström, H. Linke, G. Karlström, and A. Wacker, Phys. Rev. B **84**, 113415 (2011).
[35]P. Trocha and J. Barnaś, Phys. Rev. B **85**, 085408 (2012).
[36]G. Gómez-Silva, O. Ávalos-Ovando, M. L. Ladron de Guevara, and P. A. Orellana, J. Appl. Phys. **111**, 053704 (2012).
[37]M. L. Ladron de Guevara and P. A. Orellana, Phys. Rev. B **73**, 205303 (2006).
[38]Z. T. Jiang, Q. F. Sun, and Y. Wang, Phys. Rev. B **72**, 045332 (2005).
[39]R. Žitko and J. Bonča, Phys. Rev. Lett. **98**, 047203 (2007).
[40]Y. P. Shim, F. Delgado, and P. Hawrylak, Phys. Rev. B **80**, 115305 (2009).
[41]H. H. Fu and K. L. Yao, J. Appl. Phys. **108**, 084510 (2010).
[42]R. H. Dicke, Phys. Rev. **93**, 99 (1954).
[43]T. V. Shahbazyan and M. E. Raikh, Phys. Rev. B **49**, 17123 (1994).
[44]P. A. Orellana, M. L. Ladron de Guevara, and F. Claro, Phys. Rev. B **70**, 233315 (2004).
[45]P. A. Orellana, G. A. Lara, and E. V. Anda, Phys. Rev. B **74**, 193315 (2006).
[46]P. Trocha and J. Barnaś, J. Phys.: Condens. Matter **20**, 125220 (2008).
[47]P. Trocha and J. Barnaś, Phys. Rev. B **78**, 075424 (2008).
[48]E. Vernek, P. A. Orellana, and S. E. Ulloa, Phys. Rev. B **82**, 165304 (2010).